

A MODEL FOR ELEMENTAL CORONAL FLUX LOOPS

C. BEVERIDGE¹, D. W. LONGCOPE² and E. R. PRIEST¹

¹*Mathematical Institute, University of St. Andrews, North Haugh, St. Andrews, KY16 9SS, U.K.
(e-mail: colinb@mcs.st-and.ac.uk)*

²*Department of Physics, Montana State University, Bozeman MT59717, U.S.A.*

(Received 16 January 2003; accepted 6 May 2003)

Abstract. The photosphere possesses many small, intense patches of magnetic flux. Each of these patches (or *sources*) is connected magnetically through the corona to several sources of opposite polarity. An *elemental flux loop* consists of all of the flux joining one such source to another. We find that each source is connected to twenty other sources, on average, and that the typical flux and diameter of elemental loops in the corona are 10^{16} Mx and 200 km; there are approximately 17 separators for each source. We also model a typical large-scale coronal loop consisting of many elemental loops and determine its complex internal topology. Each upright null lies at the end of about 22 separatrices, which tend to be clustered together in trunk-like structures, analogous to river-valleys in a geographical contour map. Prone nulls correspond to saddle points, while their spines are analogous to watersheds.

1. Introduction

The magnetic energy density in the low solar corona is far larger than any other form of energy. It follows that many coronal events are driven by the magnetic field. Since magnetic loops are the fundamental building blocks of the corona (Rosner, Tucker, and Vaiana, 1978), it is natural to seek to determine their nature, including their size distribution and topology.

Coronal loops may be observed in soft X-rays and in EUV. Their size and discrete nature have been attributed to their being anchored in small-scale photospheric elements (Litwin and Rosner, 1993). An *elemental flux loop* can then be defined as comprising all the field lines anchored to a given pair of source elements.

Our aim here is to develop a model for elemental flux loops, from which we might understand their magnetic properties. A key question then is: How many photospheric elements of opposite polarity are interconnected through the corona? Since it is possible that separator reconnection (Priest and Titov, 1996; Galsgaard and Nordlund, 1997; Longcope, 1996; Galsgaard, Parnell, and Blaizot, 2000) contributes to coronal heating, it is important to find in particular the density and distribution of separators.

We model a large-scale coronal loop (a *super-loop*) anchored in unipolar areas of an active region. Each unipolar area consists of a large number of elemental



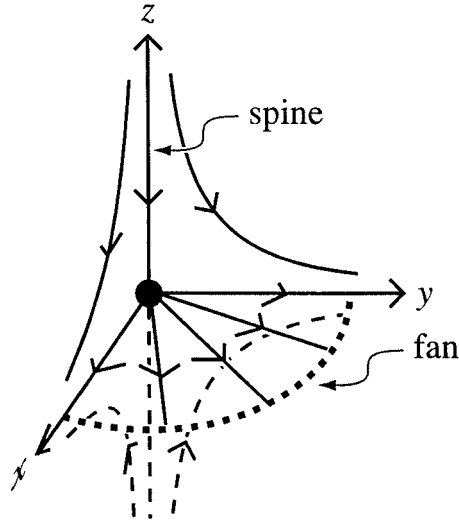


Figure 1. The field structure near a 3-dimensional positive proper radial null point marked as a *dark circle*. An isolated spine field line lies on the z -axis, directed towards the null; fan field lines diverge horizontally from the null in the $x - y$ plane.

sources, with flux $\Phi \sim 10^{17}$ Mx (Stenflo, 1994). Following Longcope and van Ballegoijen (2002), we identify the pattern of interconnections between such sources.

The boundaries of the flux domains are found by examining the *skeletons* of the null points of the magnetic field (see Priest, Bungey, and Titov, 1997). The skeleton of the field consists of the topological features of the spine and fan field lines, as shown in Figure 1, and the separators (all defined below).

A null point is a location at which the magnetic field vanishes; the local structure of null points has been extensively studied (for instance by Parnell *et al.*, 1996). In particular, the co-ordinate system can be chosen so that the first-order linear field near a magnetic null can normally be written as $\mathbf{B} = \mathbf{M} \cdot \mathbf{r}$, where $\mathbf{r} = (x, y, z)^T$ and

$$\mathbf{M} = \begin{pmatrix} \frac{\partial B_x}{\partial x} & \frac{\partial B_x}{\partial y} & \frac{\partial B_x}{\partial z} \\ \frac{\partial B_y}{\partial x} & \frac{\partial B_y}{\partial y} & \frac{\partial B_y}{\partial z} \\ \frac{\partial B_z}{\partial x} & \frac{\partial B_z}{\partial y} & \frac{\partial B_z}{\partial z} \end{pmatrix} = \begin{pmatrix} 1 & \frac{1}{2}(q - j_{\parallel}) & 0 \\ \frac{1}{2}(q + j_{\parallel}) & p & 0 \\ 0 & j_{\perp} & -(p + 1) \end{pmatrix}, \quad (1)$$

where j_{\parallel} and j_{\perp} represent components of the current parallel and perpendicular to the spine, respectively, while p and q are parameters of the potential field. We will be considering only the potential case, where j_{\parallel} and j_{\perp} are equal to zero. The solenoidal condition $\nabla \cdot \mathbf{B} = 0$ implies that the trace of the matrix \mathbf{M} in Equation (1) vanishes, and hence so does the sum of its eigenvalues. Ignoring the degenerate cases when one or more of the eigenvalues is equal to zero, it is clear

that one of the eigenvalues (λ_1) is of the opposite sign to the other two (λ_2 and λ_3). We label their corresponding eigenvectors as \mathbf{e}_1 , \mathbf{e}_2 , and \mathbf{e}_3 , respectively.

These eigenvectors are crucial to the skeleton. \mathbf{e}_1 , the eigenvector associated with the odd-signed eigenvalue, defines two isolated field lines known as *spines* (Priest and Titov, 1996). If $\lambda_1 > 0$, these are directed away from the null point, and if $\lambda_1 < 0$, they are directed towards it. Together, \mathbf{e}_2 and \mathbf{e}_3 define a *fan plane*, containing field lines which form a *separatrix surface* dividing space into regions of different connectivity. If λ_2 and λ_3 are positive, these field lines diverge from the null point; if the eigenvalues are negative, the field lines converge on the null.

Separators are field lines which begin at one null point and end at another. They can also be seen invariably as the intersections of separatrix surfaces. Since they border on four different regions of connectivity, they are prime locations for reconnection (Greene, 1988; Lau and Finn, 1990).

The null is called *positive* if λ_2 and λ_3 are both positive, or *negative* if both are negative. When all of the sources are located on a plane (the *photosphere*), there will be a population of nulls which lie in this plane, called *photospheric nulls*. If the spine of a photospheric null point lies in the plane of the sources, it is described as *prone*, whereas a photospheric null whose spine is directed vertically is called *upright*.

The numbers of sources (S), prone nulls (n_p) and upright nulls (n_u) in the photospheric plane are related by the two-dimensional Euler characteristic,

$$S + n_u = n_p + 1, \quad (2)$$

when the net flux in the source plane is non-zero (Inverarity and Priest, 1999). The properties of nulls in 3D space are governed by the 3D Euler characteristic,

$$S_+ - n_+ = S_- - n_- + q, \quad (3)$$

where S_{\pm} represents the number of positive or negative sources, n_{\pm} the number of positive or negative nulls, and q the sign of the flux imbalance ($q = 1$ if there is a net positive flux and $q = -1$ for a net negative flux).

Nulls may be created and destroyed, in accordance with these characteristics, in at least two types of local bifurcation (see Brown and Priest, 1999a), known as the *local separator* and the *local double-separator*, (or pitchfork) bifurcation. The local separator bifurcation either creates a pair of nulls where previously there were none, or destroys a pair of nulls. Equation (3) insists that they be of opposite signs, while Equation (2) implies that if the bifurcation happens in the source plane then one null must be upright and the other prone. Bifurcations in the source plane are far more common than those above or below it, and we will be concerned in this paper only with source-plane bifurcations.

The local double-separator bifurcation either creates three nulls where there was only one before, or allows three nulls to reduce to one. This is one of the mechanisms by which coronal nulls are created or destroyed, and is of no concern to us in this paper.

Additionally, in a plane consisting only of positive sources, all of the prone nulls must be positive and all of the upright nulls negative. This is because the field immediately above the plane must be directed away from it, while the spine of a positive upright null and the fan of a negative prone null would both contradict this. The converse is also true, so that negative sources give rise only to negative prone nulls and positive upright nulls.

In the first part of our analysis, we examine the topology of a source plane containing a large number of point sources, and how it varies with the distribution of flux and fraction of flux with a particular sign. In particular, we find an approximation for the number of upright nulls in each case, from which the number of prone nulls can be calculated.

In the second part, we examine the number and distribution of separators when a strictly positive region is connected to a strictly negative region. We find a large number of magnetic separators within the super-loop (roughly 17 for each source of a given polarity). These have a tendency to be clustered closely together.

Finally, we deduce that each source is connected to, on average, twenty opposing sources; this leads immediately to the conclusion that an average elemental loop will have a flux $\Phi_L \sim 10^{16}$ Mx, corresponding to a diameter of around 200 km in a coronal field of typical strength. A similar estimate is obtained by Priest, Heyvaerts, and Title (2002).

In Section 2 we outline our model, in Section 3 we discuss the topology of the source plane. Section 4 examines our results on separators, and deals with the loops themselves. We conclude in Section 5 with a discussion of our results.

2. Model

Following Longcope and van Ballegoijen (2002), we consider a magnetic super-loop with a large aspect ratio geometry, as depicted in Figure 2: the loop length is much greater than its radius, and for simplicity, we treat it as approximately straight. At each end is a boundary representing a section of the photosphere and containing small, discrete flux sources. One end represents the positive polarity of an active region and the majority of its photospheric sources are positive. Unlike Longcope and van Ballegoijen, we do not restrict ourselves to strictly unipolar source planes. The result is a *magnetic carpet* layer below the merging height (Schrijver *et al.*, 1997; Parnell, 2000; Priest, Heyvaerts, and Title, 2002). In our analysis, we assume the distance between these sources is large enough in comparison to their size that we can treat them as point sources.

We perform two numerical experiments, detailed below: the first examines the topology of the magnetic field within the source plane, which includes a determination of the proportion of upright nulls due to a given source configuration. The second examines how this topology relates to the coronal field, its separators and elemental coronal loops.

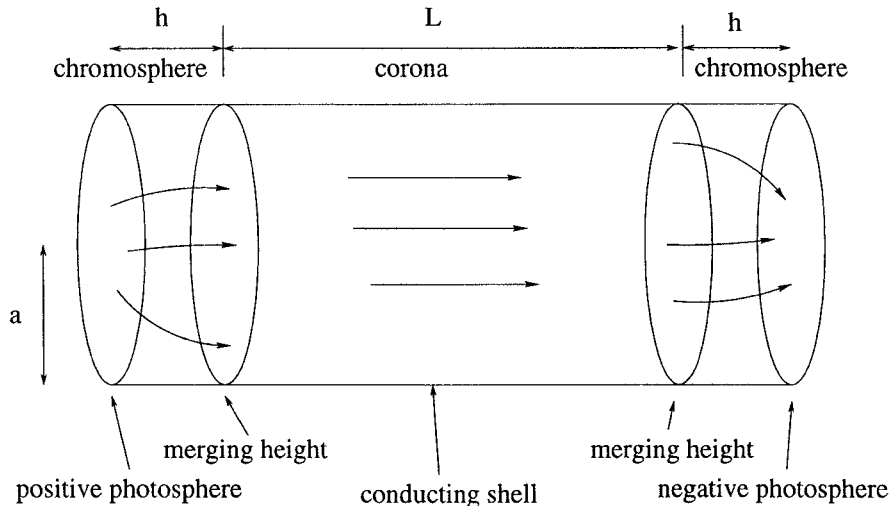


Figure 2. A straight flux loop, after Longcope and van Ballegooijen (2002). The relative dimensions have been exaggerated for clarity, whereas the model assumes a long, thin loop with a small chromosphere so that $a \ll h \ll L$.

Each calculation in the two experiments is performed by a Monte Carlo method using numerous realisations of source distributions. A single realisation consists of 1000 sources whose positions are randomly generated to produce a planar Poisson point process of unit mean density within a disk centred at the origin (Kendall and Moran, 1963; Longcope, Brown, and Priest, 2003). The mean separation of two sources is

$$\bar{r} = \int_0^{\infty} r p(r) dr,$$

where the point distribution function for unit density is

$$p(r) = 2\pi r e^{-\pi r^2},$$

and r represents the distance between nearest neighbours in units of length such that the mean density $N = 1$. This results in $\bar{r} = 0.5$.

We perform two types of calculation, by making two different assumptions about the source magnitudes. In one type all magnitudes are equal, while in the other type the magnitudes are drawn randomly from an exponential distribution. We consider these two cases in recognition of the fact that the true size distribution of fundamental flux elements is unknown. Larger magnetic elements, such as those in the quiet Sun (Schrijver *et al.*, 1997), show an exponential distribution of fluxes whose mean is $\Phi \simeq 10^{19}$ Mx. Each of these elements is, however, composed of numerous fundamental elements of typical size 10^{17} Mx.

The signs of the flux elements within a plane are chosen to produce a region with a prescribed level of *flux imbalance*, by making a fraction f of the sources

positive. In the positive end of the cylinder $f > 0.5$ while in the negative end $f < 0.5$. Since the topological properties of a magnetic field do not depend on sign, we need only consider cases with $0.5 < f \leq 1.0$.

The first series of experiments characterises the magnetic field in the source plane. A unipolar region interspersed with opposing flux elements will contain a magnetic carpet within which their field lines close. The remaining field maps through the carpet to the merging layer (and thereafter through the corona to a region of opposing polarity). To clarify this, we determine how the density of both types of photospheric null point, upright and prone, vary with flux imbalance f .

The second of our experiments will apply the topology of the photospheric field to the corona. In the model of Longcope and van Ballegoijen, the topology of the coronal field is determined entirely by the topology of the field at each merging layer, rather than at the photosphere (the coronal field is by definition unidirectional, so it maps the field lines without changing their topology). The only cases where we can approximate the merging layer topology by the photospheric topology are those without a magnetic carpet ($f = 0$ and $f = 1$). We therefore restrict our consideration to the case $f = 1$ and furthermore assume that the coronal field is unstressed, and therefore maps between merging heights without distortion.

Under these assumptions, separators above the merging height are oriented along lines parallel to the cylinder's axis. These coincide with the intersections of separatrix curves when the two merging height layers are superposed. We make the assumption that the topology of the field at the merging height is qualitatively similar to that in the source plane. In reality, the chromospheric field between the source plane and the merging height expands and adapts to fill the available space; however, we do not expect the merging height topology to be significantly different.

3. Topology of the Source Plane

In this section, we find the densities of prone and upright nulls as functions of flux imbalance f and the nature of source magnitudes. We do this by performing Monte Carlo simulations of the source planes, repeating the experiment 1000 times for each set of parameters: firstly, the strength distribution (uniform strengths or exponentially distributed) and secondly, the fraction of positively signed flux f , which we examine for f between 0.5 and 1.0 in steps of 0.1.

Each critical point of the field – each source and null point – corresponds to an extremum in the source plane of the field's scalar potential. A positive source or upright null corresponds to a maximum of the potential; a negative upright null or source corresponds to a minimum. A prone null, meanwhile, corresponds to a saddle point irrespective of its sign. The number of prone nulls is significantly larger than the number of upright nulls.

We determine the number of upright nulls by finding all the extrema of the potential. We do this using two gradient masks, one of which associates with each

TABLE I

Upright null density d_u (nulls per d area) as a function of the fraction of positive flux f , when the source strength distribution is (*left*) uniform and (*right*) exponential.

| f | d_u uniform | Exponential |
|-----|---------------------|---------------------|
| 1.0 | 0.1198 ± 0.0055 | 0.0968 ± 0.0049 |
| 0.9 | 0.0588 ± 0.0038 | 0.0468 ± 0.0034 |
| 0.8 | 0.0243 ± 0.0025 | 0.0218 ± 0.0023 |
| 0.7 | 0.0115 ± 0.0017 | 0.0095 ± 0.0015 |
| 0.6 | 0.0058 ± 0.0012 | 0.0038 ± 0.0010 |
| 0.5 | 0.0020 ± 0.0007 | 0.0018 ± 0.0007 |

point in a grid the co-ordinates of the adjacent point with the highest value, while the other does so with the lowest value. From this information, using a sufficiently fine grid, it is easy to find all of the extrema reliably.

We then use a Newton solver to find the nulls near such extrema – this also removes from our list of nulls any maxima or minima corresponding to sources – and lastly we ensure that each of the nulls is indeed an upright null by examining the alignment of its spine field line.

We average the number of upright nulls over the 1000 experiments. The results are given in Table I and Figure 3; from these, we determine the number of prone nulls from the Euler characteristic (2). We find the following relationship between the number of upright nulls (n_u), the flux (f):

$$n_u = 4.0 \times e^{-8.04f}$$

in the uniform case and

$$n_u = 3.2 \times e^{-8.04f}$$

in the exponential case.

These results show that the less mixed a region, the more numerous the upright nulls; also the uniform distribution of source strengths produces slightly more upright nulls than the exponential distribution, approximately in the proportion 5 : 4.

4. Separators and Flux Loops

In this section, we find the density and distribution of separators in a super-loop and from this calculate the average value for the size of an elemental loop. We

deduce the number of separators from the number of points where the projections of positive and negative separatrices cross. As mentioned previously, this assumes a straight coronal field so that the mapping is a simple overlay of the two topologies.

In the case where $f = 1$, none of the field lines close back into the source region. This implies there is no magnetic carpet, and we expect the topology at the merging height to be quite similar to that at the photosphere: we expect trunks to form at the merging height, but we do not expect the mapping to preserve relative areas. Since we are interested only in the topology, we assume the merging height to have the same configuration as the photosphere.

Section 3 found that the density of upright nulls in the exponential case with $f = 1$ is $d_u = 0.10$ nulls per unit area. Since this density assumed a distribution of sources with unit density, d_u also denotes the number of upright nulls per photospheric source.

From the Euler characteristic (2), we deduce the density of prone nulls to be $d_p = 1 + d_n = 1.1$. This implies that there are approximately 11 prone nulls for every upright null. Every prone null is the origin of exactly two separatrix curves within the photosphere, each of which must end at an upright null since there are no negative sources in the plane. This means that an average of about 22 separatrix field lines from surrounding prone nulls lead to each upright null.

Figure 4 shows an example of the separatrix curves connecting prone to upright nulls. It is evident from this typical view that the separatrices tend to form *trunks*, where several field lines run extremely close together – a clear example runs down the centre of the figure and ends at the upright null near (0.5, 0.5).

We next determine the locations of separators by superposing two realisations of the photospheric field, each of which is generated as described in the previous section. One of these realisations represents the positive end of a loop, the other the negative boundary. This superposition represents a mapping by way of straight coronal field lines.

Each crossing of the superposed photospheric separatrix curves is a *separator*. Figure 5 shows a piece of a superposition where the solid (respectively, dashed) curves are the separatrix curves on the positive (respectively, negative) boundary. The separators, where these lines cross, are marked by pluses.

We then count the number of separators in a central subregion measuring 10 units by 10 units, and repeat this experiment 30 times. Were the points uniformly distributed so that their counts obeyed Poisson statistics, we would expect to find $N_{\text{sep}} = d_{\text{sep}}(10^2) = 1740 \pm 42$ in our 10×10 box. Instead we count 1665 ± 461 , which varies more than an order of magnitude beyond expectation. This indicates that separators are not uniformly distributed, but tend to form in clusters. This clustering is due to the arrangement of separatrices at each boundary into trunks. Where one trunk crosses the projection of another, many separators form in a small area.

We explore the effect of clustering through a simple model in which all separators occur in clusters of size C . These clusters are themselves distributed uniformly

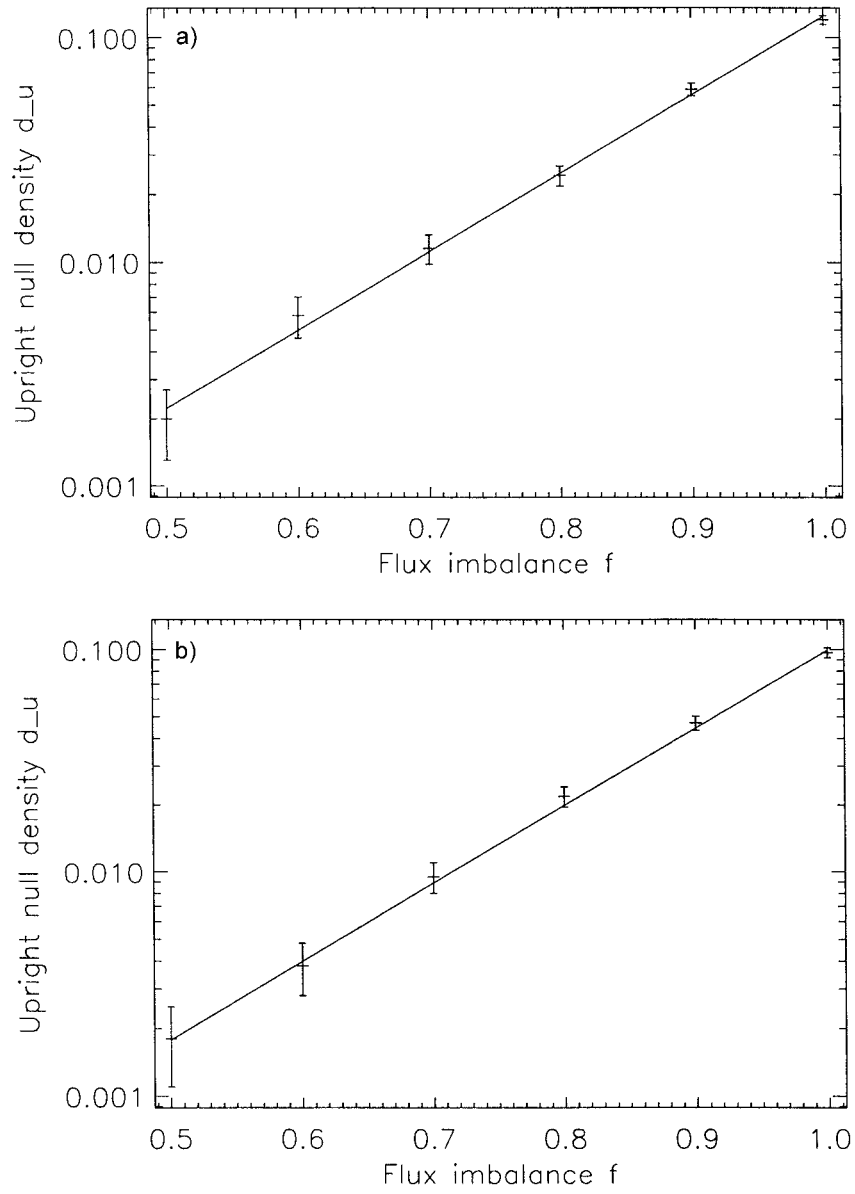


Figure 3. Plots of the flux imbalance f against the upright null density d_u when the source strength distribution is (a) uniform and (b) exponential. The *solid lines* represent our fitted curves of the form (a) $n_u = 4.0 \times e^{-8.04f}$ and (b) $n_u = 3.2 \times e^{-8.04f}$.

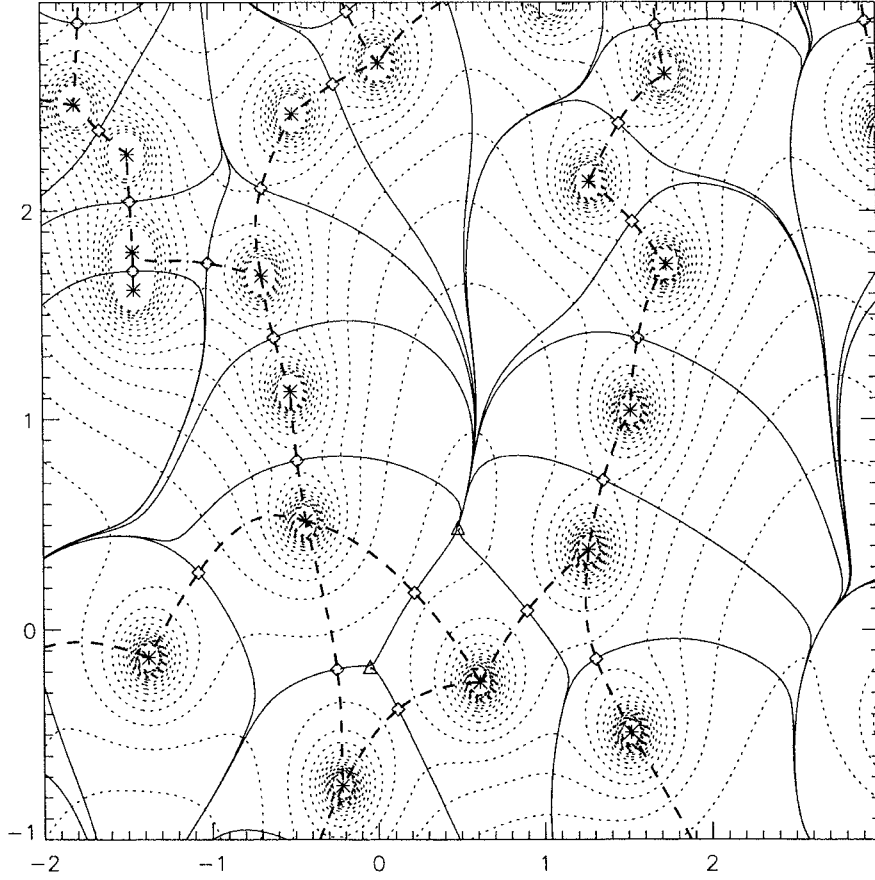


Figure 4. A part of a simulated photosphere, about 5 units by 4 units, where one unit is twice the mean separation of sources. The sources (*asterisks*) determine the positions of the prone and upright null points (*diamonds* and *triangles*, respectively). The separatrixes of prone nulls (*solid lines*) divide the plane into domains associated with a particular source. It can be seen that the separators tend to run closely together in trunks (a prime example runs down the centre of the diagram and ends at the upright null near (0.5, 0.5)). The spines (*dashed lines*) divide the plane into domains associated with a particular upright null. Also plotted are contours of the potential F where $\nabla F = \mathbf{B}$. It can be seen that path of a trunk is analogous to a river valley, while the spines are analogous to watersheds.

with density $d_C = d_{\text{sep}}/C$, where d_{sep} is the inferred separator density. A region of area A will therefore contain $\langle N_C \rangle = d_C A = d_{\text{sep}} A / C$ clusters. Trials will yield N_C counts centred on this mean with Poisson deviation $\sigma = \sqrt{\langle N_C \rangle}$. Thus the number of separators found within area A will be $N_{\text{sep}} = \langle N_{\text{sep}} \rangle \pm \sqrt{\langle N_{\text{sep}} \rangle} \sqrt{C}$. Our results are consistent with a cluster size $C \simeq 128$, which would occur at the intersection of two trunks with eleven separators each. Figure 6 shows this prediction against the actual results: in the lowest 70%, the prediction matches the results very well, although at the high end of the scale we consistently find more separators than we predict.

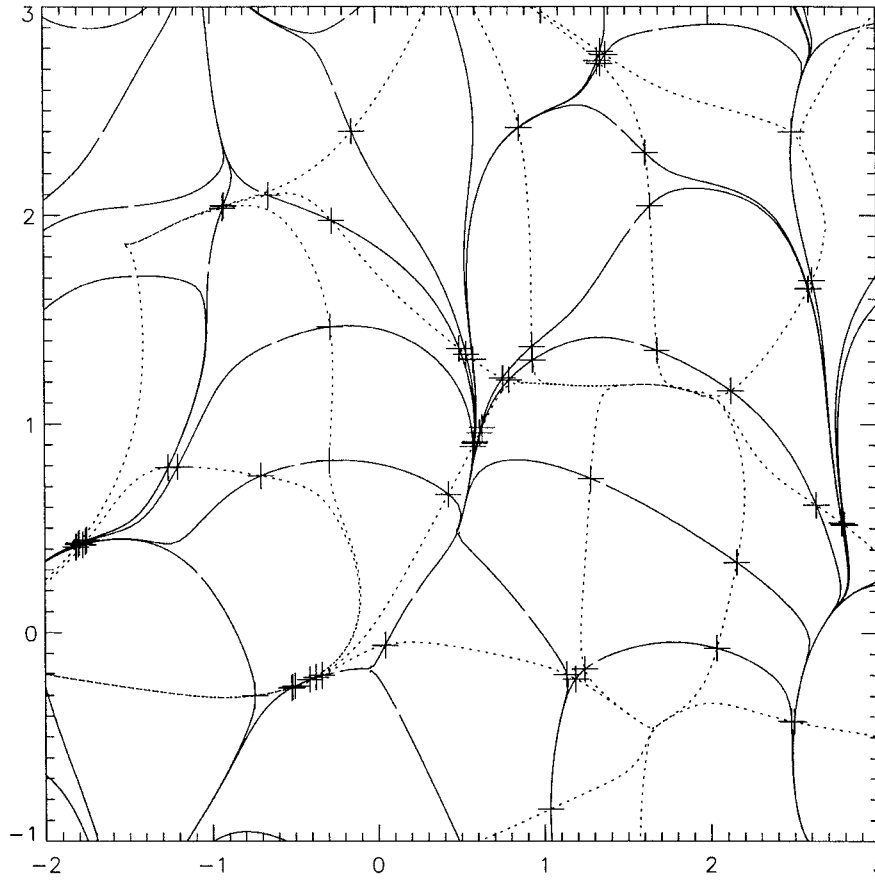


Figure 5. A part of two overlaid topologies, about 5 units by 4 units. The *solid lines* represent the separatrixes of one photosphere, the *dotted lines* those of the other. The *crosses*, where these meet, mark separators. Where two trunks cross, a large number of separators occur in a tiny area.

Given that there are around 1.1 prone nulls per unit area and each prone null has exactly two separatrix field lines in the plane, each separatrix surface contains an average of around $17.4/2.2 \simeq 8$ separators.

As for the flux domains, we know there are d_{sep} separators per unit area, and hence in an area with S sources, a total of $n_{\text{sep}} = d_{\text{sep}}S$. In an approach similar to Longcope and Klapper (2002), we therefore apply Euler's theorem:

$$f = e - v + 2, \quad (4)$$

where f represents faces, e edges and v vertices, to the superposition of two boundaries.

In the superposition, every face represents a flux domain, so $f = n_d$.

We count as a vertex all photospheric nulls and separators, so we have $v = 2(n_p + n_u) + n_{\text{sep}}$ vertices. Edges are constituted by the parts of field lines joining

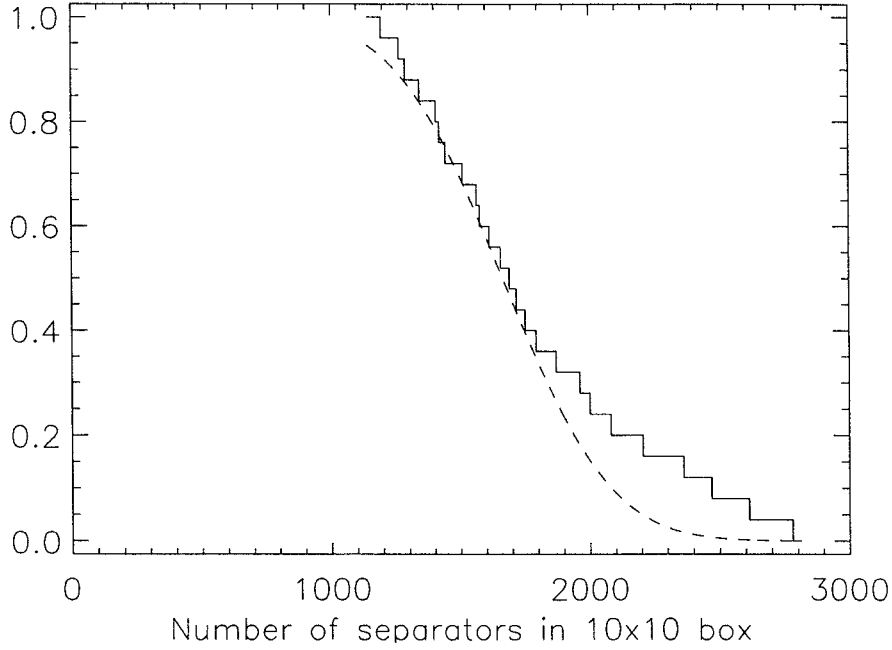


Figure 6. Cumulative histogram of separator number n_{sep} (solid line) against prediction (dashed curve). There is very good agreement for the lowest 70%, although we find more separators than predicted at higher values.

vertices: that is, connecting two separators, two nulls, or a null and a separator. There are $e = 4n_p + 2n_{\text{sep}}$ edges.

Equation (4) then becomes

$$n_d = 2n_p - 2n_u + n_{\text{sep}} + 2,$$

where n_d is the number of domains. However, $n_p - n_u = S$; moreover, in a large area, we can ignore the 2. So,

$$n_d \sim (2 + d_{\text{sep}})S.$$

With our value of $d_{\text{sep}} = 18.1$, we find $n_d = 20.1 S$; on average, then, each source connects to about twenty opposing sources.

Stenflo-sized elements have a flux of $\Phi \sim 10^{17}$ Mx (Stenflo, 1994), so our loops have a flux $\Phi_L \sim 10^{16}$ Mx. Taking a typical coronal magnetic field strength of 10 G, we find an average diameter for each flux loop of around 200 km, corresponding to 0.2 arc sec. This is a little finer than the limit of TRACE resolution, and similar to the estimate of Priest, Heyvaerts, and Title (2002). It must be noted, however, that due to the propensity of separators to form trunks, many of these flux loops are expected to be very thin indeed and to have very little flux.

5. Conclusions

The *magnetic carpet* – the arrangement of connections between flux sources in the solar photosphere – is an incredibly complicated, and forever-changing, structure (e.g., Schrijver *et al.*, 1997; Parnell, 2000; Simon, Title, and Weiss, 2001). New sources are constantly emerging as old sources disappear; others coalesce to form larger sources, while others divide into smaller ones. Yet others come together and cancel each other out.

An important aspect of studying the phenomena due to the carpet is to determine in detail the topology due to its sources. Much progress has been made, both in the examination of small numbers of sources (for instance, the three-source case has been completely classified (Brown and Priest, 1999a) and a start has been made on four sources – in a balanced scenario (Beveridge, Priest, and Brown, 2002) and in unbalanced cases (Brown and Priest, 1999b, 2001)) as well as in discussion of general concepts (Longcope, 2001).

Our analysis approaches the problem from a different angle, with a direct physical application. It is one of the first studies to predict flux loop sizes from a theoretical standpoint.

We find that the separatrix surfaces in the photospheric planes have a tendency to form *trunks* where many separators lie close together. One way to understand this is to consider the magnetic potential F , where

$$\mathbf{B} = \nabla F.$$

Supposing all of the sources to be positive, F has a local maximum at each source. At each prone null in the source plane, the potential has a saddle point, and at each upright null, F has a local minimum. By analogy to a geographical contour map, these trunks can be seen to follow valleys of the potential. This analogy can be extended to include the spines, which trace the watersheds of the potential landscape, as can be seen in Figure 4.

The bottom of a potential valley is the location of an upright null and so the shape of a valley nearby is given by the potential, which can be calculated from the magnetic field equation (1) to give

$$F = \frac{x^2}{2} + qxy + \frac{py^2}{2} - (p+1)z.$$

One explanation for the tendency for the separatrices of surrounding nulls to form a trunk as they approach such a null could perhaps be that the fan field lines at a generic upright null are not equally spaced but are aligned preferentially towards one of the fan eigenvectors (in fact, the one corresponding to the larger eigenvalue).

We superpose two photospheric planes as an approximation to a straight super-loop. The intersections correspond to separators, while the spaces in the network are the elemental flux loops.

We find that many of these loops will carry very little flux – where trunks intersect, a large number of loops and separators will occur in a small area. We expect this phenomenon to be replicated at the merging height, and suspect that direct methods may find fewer connections – it is unlikely that tracing field lines from sources would find all of the flux loops that we do.

We now plan to extend this analysis of model fields to more realistic ones by extrapolating MDI data. There remain, however, many questions even in this simplified model: is separator heating more or less efficient than the separatrix heating proposed in the Coronal Tectonics Model (Priest, Heyvaerts, and Title, 2002)? Why exactly do the trunks form, and what do they represent? What happens physically when a large number of separators are clustered together in a tiny space? Does reconnection in such clusters contribute significantly to coronal heating?

Acknowledgements

The authors are grateful to the UK Particle Physics and Astronomy Research Council for financial support, and to Dr Daniel Brown for useful discussions.

References

- Beveridge, C., Priest, E. R., and Brown, D. S.: 2002, *Solar Phys.* **209**, 333.
 Brown, D. S. and Priest, E. R.: 1999a, *Proc R. Soc. London* **A455**, 3931.
 Brown, D. S. and Priest, E. R.: 1999b, *Solar Phys.* **190**, 25.
 Brown, D. S. and Priest, E. R.: 2001, *Astron. Astrophys.* **367**, 339.
 Galsgaard, K. and Nordlund, Å.: 1997, *J. Geophys. Res.* **102**, 231.
 Galsgaard, K., Parnell, C. E., and Blaizot, J.: 2000, *Astron. Astrophys.* **362**, 383.
 Greene, J. M.: 1988, *J. Geophys. Res.* **93**, 8583.
 Inverarity, G. and Priest, E. R.: 1999, *Solar Phys.* **186**, 99.
 Kendall, M. G. and Moran, P. A. P.: 1963, *Geometrical Probability*, Charles Griffin and Co., London.
 Lau, Y. -T. and Finn, J. M.: 1990, *Astrophys. J.* **350**, 672.
 Litwin, C. and Rosner, R.: 1993, *Astrophys. J.* **412**, 375.
 Longcope, D. W.: 2001, *Phys. Plasmas* **8**, 5277.
 Longcope, D. W.: 1996, *Solar Phys.* **169**, 91.
 Longcope, D. W. and Klapper, I.: 2002, *Astrophys. J.* **579**, 468.
 Longcope, D. W. and van Ballegoijen, A. A.: 2002, *Astrophys. J.* **578**, 573.
 Longcope, D. W., Brown, D. S., and Priest, E. R.: 2003, submitted.
 Parnell, C. E.: 2000, *Solar Phys.* **200**, 23.
 Parnell, C. E., Smith, J. M., Neukirch, T., and Priest, E. R.: 1996, *Phys. Plasmas* **3**, 759.
 Priest, E. R. and Titov, V. S.: 1996, *Phil. Trans. R. Soc. London* **A354**, 2951.
 Priest, E. R., Bungey, T. N., and Titov, V. S.: 1997, *Geophys. Astrophys. Fluid Dynamics* **84**, 127.
 Priest, E. R., Heyvaerts, J. F., and Title, A. M.: 2002, *Astrophys. J.* **576**, 533.
 Rosner, R., Tucker, W. H., and Vaiana, G. S.: 1978, *Astrophys. J.* **220**, 643.
 Schrijver, C. J., Title, A. M., van Ballegoijen, A. A., Hagenaar, H. J., and Shine, R. A.: 1997, *Astrophys. J.* **487**, 424.
 Simon, G. W., Title, A. M., and Weiss, N. O.: 2001, *Astrophys. J.* **561**, 427.
 Stenflo, J. O.: 1994, *Solar Magnetic Fields: Polarized Radiation Diagnostics*, Kluwer Academic Publishers, Dordrecht, Holland.